Rare Metal Materials and Engineering
Volume 54, Issue 8, August 2025
Available online at www.rmme.ac.cn

Science Press

Cite this article as: Zhao Yunxing, Yu Jingyi, Ma Dexin, et al. Effect of Withdrawal Rate on Non-uniform Distribution of Eutectic in Ni-based Single Crystal Superalloy Castings[J]. Rare Metal Materials and Engineering, 2025, 54(08): 1934-1939. DOI: https://doi.org/10.12442/j.issn.1002-185X.20240435.

ARTICLE

Effect of Withdrawal Rate on Non-uniform Distribution of Eutectic in Ni-based Single Crystal Superalloy Castings

Zhao Yunxing[1,3], Yu Jingyi[1,2], Ma Dexin[1,3], Huang Zaiwang[1,2]

[1] State Key Laboratory of Powder Metallurgy, Central South University, Changsha 410083, China; [2] Powder Metallurgy Research Institute, Central South University, Changsha 410083, China; [3] Wedge Central South Research Institute Co., Ltd, Shenzhen 518045, China

Abstract: The microstructure of single crystal superalloy is relatively simple, consisting primarily of γ dendrites and γ/γ' eutectics. During the directional solidification process of Ni-based single crystal superalloys, withdrawal rate is a critical parameter affecting the spatial distribution of γ/γ' eutectic along gravity direction. The results show that the γ/γ' eutectic fraction of the upper platform surface is always higher than that of the lower one, regardless of withdrawal rate. As the withdrawal rate decreases, there is a significant increase in γ/γ' eutectic fraction on the upper surface, while it decreases on the lower surface. The upward accumulation of γ/γ' eutectic becomes more severe as the withdrawal rate decreases. It is also found that the percentage of Al+Ta is positively correlated with the γ/γ' eutectic fraction. Thermo-solute convection of Al and Ta solutes in the solidification front is the prime reason for the non-uniform distribution of eutectic. The non-uniform distribution of γ/γ' eutectic cannot be eliminated even after subsequent solution heat treatment, resulting in excess eutectic on the upper surface and thus leading to the scrapping of the blade.

Key words: Ni-based single crystal superalloy; eutectics; withdrawal rate; thermo-solute convection

1 Introduction

There are many types of high-temperature materials, such as intermetallic compounds, carbide materials, and superalloys. These materials are extensively utilized in various industrial applications due to their exceptional performance at elevated temperatures[1–5]. Ni-based single crystal (SX) superalloys are widely used in high-pressure turbine blades and vanes of aero-engine owing to their excellent creep, oxidation, and corrosive resistances at elevated temperature up to 1150 ℃[5–6]. These desirable properties primarily originate from two microstructural advantages: (1) solid solution strengthening via the addition of 15wt% – 20wt% refractory elements, such as rhenium (Re), tungsten (W), molybdenum (Mo), and tantalum (Ta); (2) precipitation hardening due to the presence of nearly 70% γ' precipitates coherent with an $L1_2$ structure, achieved by alloying elements Al, Ta, and Ti. During directional solidification, γ phase commences to solidify and heavy elements such as Re and W are segregated towards the dendrite core, while light elements Al, Ti, and Ta are rejected and enriched in the interdendritic liquid that solidifies in final stage. As a result, there is an upward flow of light solutes, such as Al and Ti which induce thermo-solute convection under the effect of gravity[7–10]. Once these light elements are accumulated in the upper area, a higher fraction of γ/γ' eutectics will be formed. This justification can be supported by the fact that the volume fraction of γ/γ' eutectic increases in higher-generation Ni-based SX superalloys, exceeding 10% in third-generation alloys[11–13].

In addition, the solidification parameters play a crucial role in influencing the size, spatial distribution, volume fraction, and morphologies of γ/γ' eutectic[14–20]. Recent research has reported that the volume fraction of γ/γ' eutectic is higher on the outside surface compared to the inner surface after solidification of Ni-based SX superalloys. This phenomenon is attributed to the contraction of ceramic molds during cooling, resulting in compressive stress that drives the eutectic liquid towards outside surface[21–23]. However, this conclusion has been challenged by recent experimental observations as no apparent difference in eutectic fraction is observed from inside

Received date: July 17, 2024
Foundation item: Shenzhen Science and Technology Program (JSGG20220831092800001)
Corresponding author: Huang Zaiwang, Ph. D., Professor, State Key Laboratory of Powder Metallurgy, Central South University, Changsha 410083, P. R. China, E-mail: huangzaiwang@csu.edu.cn

to outside. On the contrary, several experimental results have revealed the accumulation behavior of γ/γ' eutectic in the upper area of castings[24–25]. The mechanism is attributed to thermo-solute convection of solutes Al, Ti, and Ta driven by gravity, which can induce long-distance transport of light solutes, and chimney-like plumes have been directly recorded by X-ray radioscopy in Ga-In, Al-Cu, and CMSX-4 alloys[26–30].

In this research, the effect of withdrawal rate on the formation, evolution, and distribution of eutectics in a third-generation Ni-based SX superalloy was investigated. The experimental observations clearly demonstrate that eutectic fraction is strongly dependent on the withdrawal rate during directional solidification. Gravity-induced solute convection of Al, Ti, and Ta is the prime reason for this behavior, which has been validated by compositional analysis.

2 Experiment

The nominal composition of a novel third-generation Ni-based SX superalloy (WZ30) is listed in Table 1. The alloy ingot was prepared by vacuum induction melting, and SX plates with three platforms were designed, as shown in Fig. 1. Normally, the maximum withdrawal rate for directional solidification of SX superalloy is approximately 3 mm/min. Consequently, SX test plates were fabricated by Bridgman method (ALD GmbH, Germany) using three withdrawal rates of 0.3, 1.0, and 3.0 mm/min, respectively. Solution heat treatment was performed via the processing of 1280 °C/9 h + 1310 °C/7.5 h+1325 °C/9.5 h+1340 °C/6 h+air cooling. The samples (longitudinal and vertical planes) were cut from the middle flange, ground and polished by standard metallography process, and then chemically etched with a solution consisting of 33% HNO_3+33% acetic acid+33% H_2O+1% HF. Scanning electron microscope (SEM, FEI Quanta 650) was used to observe microstructures.

Table 1 Nominal composition of a third-generation Ni-based SX superalloy WZ30 (wt%)

Cr	Co	W	Mo	Al	Ti	Ta	Re	Nb	Ni
3.5	6.0	6.5	0.4	5.8	0.15	8.0	4.95	0.1	Bal.

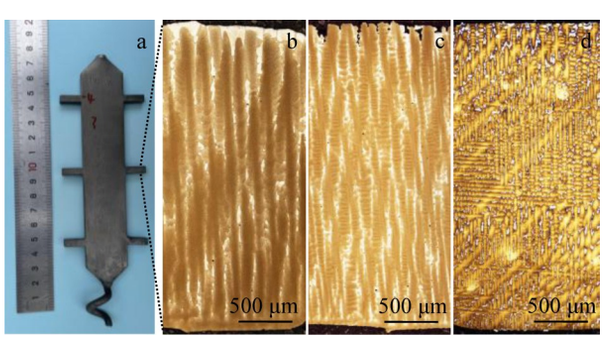

Fig.1 Ni-based SX plate with platforms (a) and microstructures of dendrites and eutectics under different withdrawal rates (b–d): (b) 0.3 mm/min, (c) 1.0 mm/min, and (d) 3.0 mm/min

3 Results and Discussion

Fig. 1b–1d show the microstructures of entire platform from bottom to top after directional solidification using three withdrawal rates, in which the dark dendrites are γ phases and the bright white ones are γ/γ' eutectics[5,13]. When the withdrawal rate is 0.3 mm/min (Fig. 1b), the primary spacing between γ dendrites is large and the secondary dendrites are rarely observed. The volume fraction of γ/γ' eutectics significantly increases from bottom to top regions. When the withdrawal rate increases to 1.0 mm/min (Fig. 1c), the spacing of primary dendrites decreases and secondary dendrites are readily observed, in contrast with Fig. 1b. The non-uniform distribution of γ/γ' eutectic can still be observed, while their average sizes are obviously decreased, especially in the upper area. As the withdrawal rate is further increased to 3.0 mm/min, the primary dendrite spacing is further decreased and the secondary dendrites become more developed. Meanwhile, the size of the γ/γ' eutectics in the upper area is also further decreased.

To further verify the observations, the microstructures of the bottom and top surfaces of the same platform were observed. When the withdrawal rate is 0.3 mm/min (Fig. $2a_1$ and $2a_2$), the microstructural growth is dominated by primary dendrites, while the growth of secondary and tertiary dendrites is suppressed. In this case, the formed pattern is similar to the cellular structure. The γ/γ' eutectics observed on the top surface (Fig. $2a_1$) exhibit irregular shapes and the average size is hundreds of micrometers, in contrast to the tiny γ/γ' eutectic on the bottom surface (Fig. $2a_2$). As the withdrawal rate is increased to 1.0 mm/min, there is a noticeable refinement in the size of primary dendrite and γ/γ' eutectic on the top surface (Fig. $2b_1$). However, on the bottom surface (Fig. $2b_2$), eutectics are present with an average size smaller than that on the top surface. This trend becomes even more obvious when the withdrawal rate is accelerated to 3.0 mm/min, as shown in Fig. $2c_1$ and $2c_2$. Due to the higher withdrawal rate, there is less time for solidification and thermo-solute convection. Therefore, it is anticipated that there will be a more uniform distribution of solutes such as Al, Ta, and Ti from the bottom to the top.

To quantify the volume fraction of γ/γ' eutectics on the bottom and top surfaces under different withdrawal rates, the eutetic fractions were measured, as listed in Table 2. As the withdrawal rate decreases from 3.0 mm/min to 1.0 mm/min and then to 0.3 mm/min, the γ/γ' eutectic fractions on the top surfaces increase from 15.13vol% to 15.78vol% and 23.43vol% , while the values on bottom surfaces decrease from 10.3vol% to 6.19vol% and 0.34vol% , respectively. Fig. 3a shows the dependence of γ/γ' eutectic fractions of the bottom and top surfaces on withdrawal rates. As the withdrawal rate increases, the volume fraction of γ/γ' eutectic decreases on the top surface but increases on the bottom surface, indicating that as the withdrawal rate decreases, the upward accumulation of γ/γ' eutectic becomes more severe.

Moreover, the average composition on the top and bottom

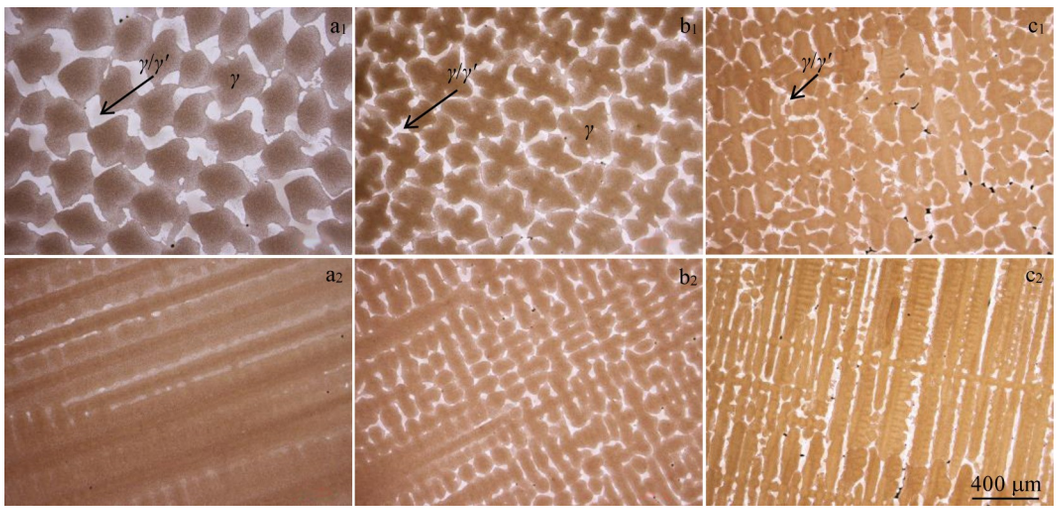

Fig.2 Microstructures of top (a_1–c_1) and bottom (a_2–c_2) surfaces of the as-cast platform under different withdrawal rates: (a_1–a_2) 0.3 mm/min, (b_1–b_2) 1.0 mm/min, and (c_1–c_2) 3.0 mm/min

Table 2 Eutectic fraction on the bottom and top surfaces under different withdrawal rates

Withdrawal rate/ mm·min^{-1}	Position	Field 1/ vol%	Field 2/ vol%	Field 3/ vol%	Field 4/ vol%	Field 5/ vol%	Average/ vol%	Average ratio (top/bottom)
3.0	Top	15.20	16.40	14.59	14.66	14.8	15.13	1.47
	Bottom	11.25	8.25	8.86	10.85	12.29	10.30	
1.0	Top	14.64	17.51	16.22	15.67	14.86	15.78	2.55
	Bottom	6.06	7.03	5.92	4.51	7.43	6.19	
0.3	Top	25.51	21.97	27.10	22.06	20.49	23.43	68.91
	Bottom	0.65	0.20	0.15	0.38	0.33	0.34	

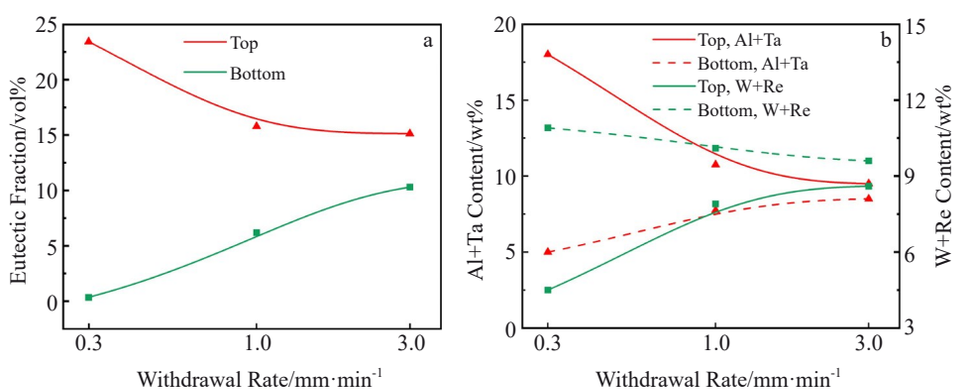

Fig.3 Dependence of γ/γ' eutectic fraction on withdrawal rates (a); compositional variation of Al+Ta and W+Re with withdrawal rates (b)

surfaces of the samples under different withdrawal rates were measured, and the results are listed in Table 3. In SX superalloys, W+Re is segregated to the dendrite core, forming γ phase, while Al+Ta is segregated to the interdendritic region, forming γ/γ' eutectic[8,12,17]. Due to different segregation behavior of alloying elements, especially W+Re and Al+Ta, their contents exhibit significant variations along the solidification direction. When the withdrawal rate is 0.3 mm/min, the Al+Ta content increases from 14.0% on the bottom surface to 19.2wt% on the top surface, corresponding to a decrease in W+Re content from 10.9wt% to 4.5wt%. With increasing the withdrawal rate, the difference of both Al+Ta and W+Re contents between the bottom and top surfaces of the platform decreases. It is clear that the content of Al+Ta on the top surface is always higher than that on the bottom surface, and the difference becomes larger with decreasing the withdrawal rate. In contrast, the content of W+Re on the top surface is invariably lower than that on the bottom surface, and decrease in withdrawal rate leads to larger difference between top and bottom surfaces. Noteworthy, other elements are more uniformly distributed along solidification direction.

Based on observations above, the distribution of γ/γ'

Table 3 Average composition of top and bottom surfaces of samples under different withdrawal rates (wt%)

Withdrawal rate/ mm·min^{-1}	Position	Al+Ta/ wt%	W+Re/ wt%	Top/ bottom (Al+Ta)	Top/ bottom (W+Re)
3.0	Top	15.8	8.6	1.03	0.90
	Bottom	15.4	9.6		
1.0	Top	16.3	7.9	1.08	0.78
	Bottom	15.1	10.1		
0.3	Top	19.2	4.5	1.37	0.41
	Bottom	14.0	10.9		

eutectics is apparently different along solidification direction. The growth mechanisms of dendrite and γ/γ' eutectic can be categorized into three stages. In the initial stage, as the platform enters the cold zone and the temperature of the bottom platform area reaches the liquidus point, γ dendrites form and grow horizontally in the maximum temperature gradient direction (dense horizontal dendrites on the bottom surfaces in Fig. 1 and Fig. 2)[31–32]. At this moment, the content of Al+Ta in residual liquid is low and convection is weak, so the volume fraction of eutectics is small. After the completion of horizontal dendrites growth, the secondary dendrites originating from preformed horizontal dendrites will vertically grow (parallel to gravity direction) and become gradually coarse to form new primary dendrites. At this stage, withdrawal rate controls the growth rate and size of primary dendrite, the formation of new secondary dendrite[33–36], as well as the speed of thermo-solute convection. When the withdrawal rate is reduced, the growth rate (V_d) of primary dendrites decreases accordingly, leading to simultaneous suppression of the growth of secondary dendrites and resulting in peritectic-like microstructure[37–39]. As previously stated, a slower solidification process allows for sufficient time for thermo-solute convection, especially when secondary dendrites are not present (Fig. 4a). With increasing the withdrawal rate (Fig. 4b and 4c), the primary dendrites exhibit rapid growth and a reduction in size, accompanied by the growth and coarsening of secondary and tertiary dendrites, which contributes to the resistance of thermo-solute convection.

Finally, once the dendrite tips are in contact with the top surface, dendrite growth is stopped, and solute accumulation controls the final stage of solidification. Still, the size and volume fraction of γ/γ' eutectics on the top surface is dependent on the withdrawal rate.

In order to explore the potential for eliminating the non-uniform distribution of γ/γ' eutectic through solution heat treatment, the microstructure of both top and bottom surfaces of the platform after standard solution heat treatment under different withdrawal rates are presented in Fig. 5. On the bottom surface, the γ/γ' eutectics are completely solutioned after standard heat treatment. In contrast, residual γ/γ' eutectic still exists on the top surface of all samples, and the amount of residual γ/γ' eutectic increases with decreasing the withdraw rate. In Fig. 5, all samples exhibit a significant amount of porous structure after solution heat treatment. These pores are

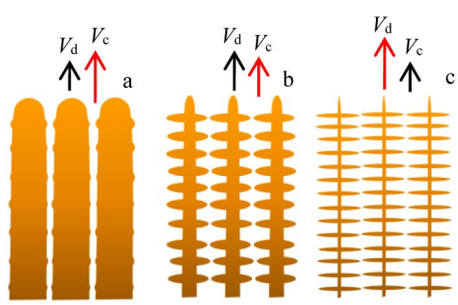

Fig.4 Schematics of dendrite growth and its dependence on thermo-solute convection under different withdrawal rates (V_c denotes thermo-solute convection rate)

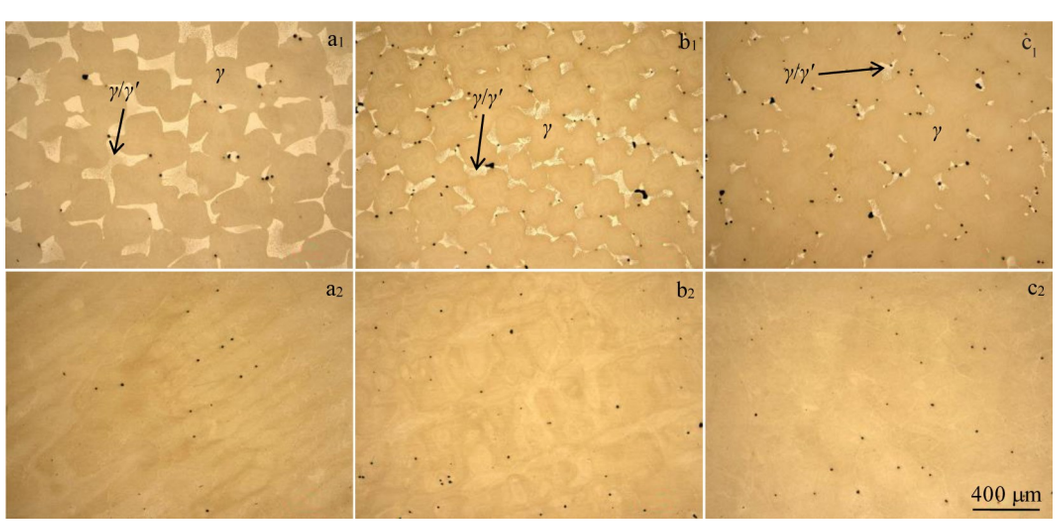

Fig.5 Microstructures of top (a_1–c_1) and bottom (a_2–c_2) surfaces after heat treatment under different withdrawal rates: (a_1–a_2) 0.3 mm/min, (b_1–b_2) 1.0 mm/min, and (c_1–c_2) 3.0 mm/min

Table 4 Residual γ/γ' eutectic fraction on the bottom and top surfaces under different withdrawal rates after heat treatment

Withdrawal rate/mm·min^{-1}	Position	Field 1/vol%	Field 2/vol%	Field 3/vol%	Field 4/vol%	Field 5/vol%	Average/vol%
3	Top	2.86	2.37	2.51	2.64	2.45	2.57
	Bottom	0	0	0	0	0	0
1	Top	8.27	7.86	7.45	8.34	8.52	8.09
	Bottom	0	0	0	0	0	0
0.3	Top	14.70	13.92	15.11	14.38	14.82	14.59
	Bottom	0	0	0	0	0	0

attributed to the micro-loose structure formed during directional solidification and the microscopic pores generated during the solid solution process.

The fractions of residual γ/γ' eutectic of the heat-treated samples were measured, and the results are shown in Table 4. The average fractions of residual γ/γ' eutectic are measured to be 2.57vol%, 8.09vol%, and 14.59vol% at withdrawal rates of 3.0, 1.0, and 0.3 mm/min, respectively. Similar to the γ/γ' eutectic distribution behavior, the residual γ/γ' eutectic fraction increases on the top surface as the withdrawal rate decreases. Comparing the results of both as-cast and heat-treated alloys, it is observed that eutectic solutioning occurs during heat treatment, and its kinetics is dependent on temperature, time, volume fraction, composition, etc. In general, the fraction of residual γ/γ' eutectic in Ni-based SX superalloys is generally controlled to be less than 3vol%. Therefore, greater emphasis must be placed on the non-uniform distribution of γ/γ' eutectic as the scrappage rate of SX blades is directly related to it.

4 Conclusions

1) Three withdrawal rates are employed to investigate their effects on the non-uniform distribution of γ/γ' eutectic. Under different withdrawal rates, the eutectic fraction at the upper area is always higher than that of the lower one. With decreasing the withdrawal rate, eutectic fraction at the upper area increases but decreases at the lower area.

2) Significant enrichment of Al+Ta is observed at the upper area due to thermo-solute convection, leading to a non-uniform distribution of γ/γ' eutectic along the solidification direction.

3) The non-uniform distribution behavior of γ/γ' eutectic can increase the risk of blade scrappage even after solution heat treatment.

References

1 Pan Y, Yang F H. *Journal of Materials Research and Technology*[J], 2024, 28: 381

2 Pan Y. *Journal of Materials Research and Technology*[J], 2023, 26: 8813

3 Pan Y. *International Journal of Refractory Metals and Hard Materials*[J], 2024, 121: 106676

4 Pan Y, Zhu J X. *Vacuum*[J], 2024, 225: 113242

5 Reed R C. *Superalloys: Fundamentals and Applications*[M]. London: Cambridge University Press, 2006

6 Koizumi Y, Kobayashi T, Yokokawa T *et al*. *Superalloys 2004*[C]. Pennsylvania: TMS, 2004: 35

7 Cheng Yuan, Zhao Xinbao, Yue Quanzhao *et al*. *Rare Metal Materials and Engineering*[J], 2023, 52(7): 2599

8 Wang Fu, Ma Dexin, Samuel Bogner *et al*. *Journal of Alloys and Compounds*[J], 2015, 647: 528

9 Zhao X B, Liu L, Zhang W G *et al*. *Materials Letters*[J], 2009, 63(30): 2635

10 Kumar M S, Malte L, Steffen N *et al*. *Scripta Materialia*[J], 2018, 157: 62

11 Zhao Yunxing, Ma Dexin, Xu Weitai *et al*. *Rare Metal Materials and Engineering*[J], 2023, 52(3): 1162 (in Chinese)

12 Seo S M, Lee J H, Yoo Y S *et al*. *Metallurgical and Materials Transactions A*[J], 2011, A42: 3150

13 Walston W S, O'Hara K S, Ross E W *et al*. *Superalloys 1996*[C]. Pennsylvania: TMS, 1996: 27

14 Wang F, Ma D X, Zhang J *et al*. *Journal of Crystal Growth*[J], 2014, 389: 47

15 Wang F, Ma D X, Zhang J *et al*. *Materials Characterization*[J], 2015, 10: 20

16 Alireza M, Mohamad F. *Materials Characterization*[J], 2022, 194: 112449

17 Warnken N, Ma D X, Mathes M *et al*. *Materials Science and Engineering A*[J], 2005, 413–414: 267

18 Souza N D, Dong H B. *Scripta Materialia*[J], 2007, 56(1): 41

19 Souza N D, Lekstrom M, Dai H J *et al*. *Materials Science and Technology*[J], 2007, 23(9): 1085

20 Ma Dexin, Wang Fu. *China Foundry*[J], 2019, 68(12): 1342

21 Brewster G, Dong H B, Green N R *et al*. *Metallurgical & Materials Transactions B*[J], 2008, 39(1): 87

22 Cao L, Yao L, Zhou Y Z *et al*. *Journal of Materials Science & Technology*[J], 2017, 4: 39

23 Cao L, Zhou Y, Jin T *et al*. *Journal of Materials Science & Technology*[J], 2017, 33(11): 84

24 Ma Dexin, Zhao Yunxing, Xu Weitai *et al*. *Acta Metallurgica Sinica*[J], 2021, 57(12): 1539 (in Chinese)

25 Ma Dexin, Zhao Yunxing, Wei Jianhui *et al*. *Chian Foundry*[J], 2021, 70(11): 1302

26 Boden S, Eckert S, Willers B *et al*. *Metallurgical and Materials Transactions A*[J], 2008, 39A: 613

27 Natalia S, Stephan B, Gunter G *et al*. *Metallurgical and Materials Transactions A*[J], 2013, 44A: 3797

28 Mathiesen R H, Arnberg L, Bleuet P *et al*. *Metallurgical and Materials Transactions A*[J], 2006, 37(8): 2515
29 Mathiesen R H, Arnberg L. *Acta Materialia*[J], 2005, 53(4): 947
30 Reinhart G, Grange D, Khalil L A *et al*. *Acta Materialia*[J], 2020, 194: 68
31 Ma Dexin, Wang Fu, Sun Hongyuan *et al*. *China Foundry*[J], 2019, 68(6): 558
32 Ma Dexin. *Acta Metallurgica Sinica*[J], 2015, 51(10): 1179 (in Chinese)
33 Qi Yongshun, Li Fengwen, Xuan Weidong *et al*. *Shanghai Metals*[J], 2022, 44(3): 65 (in Chinese)
34 Li Jinguo, Wang Zhen, Jin Tao *et al*. *Materials for Mechanical Engineering*[J], 2002(4): 17 (in Chinese)
35 Jin Tao, Li Jinguo, Zhao Nairen *et al*. *Journal of Materials Engineering*[J], 2002(3): 36 (in Chinese)
36 Liu Lirong, Mao Liang, Chen Lijia *et al*. *Rare Metal Materials and Engineering*[J], 2011, 40(12): 2212 (in Chinese)
37 Hu Zhuangqi. *Principle of Metal Solidification*[M]. Beijing: China Machine Press, 1992 (in Chinese)
38 Rutter J W, Chalmers B. *Canadian Journal of Physics*[J], 1953, 31: 15
39 Quested P N, Mclean M. *Materials Science and Engineering*[J], 1984, 65(1): 171

抽拉速率对单晶铸件中共晶组织不均匀分布的影响

赵运兴[1,3]，于静毅[1,2]，马德新[1,3]，黄再旺[1,2]
(1. 中南大学 粉末冶金国家重点实验室，湖南 长沙 410083)
(2. 中南大学 粉末冶金研究院，湖南 长沙 410083)
(3. 深圳市万泽中南研究院有限公司，广东 深圳 518045)

摘　要：单晶高温合金的微观结构相对简单，主要由γ枝晶和γ/γ'共晶组成。在镍基单晶高温合金的定向凝固过程中，抽拉速率是影响γ/γ'共晶沿重力方向分布的关键参数。结果表明，无论抽拉速率如何，铸件平台上表面的γ/γ'共晶比例始终高于平台下表面。且随着抽拉速率的降低，上表面中γ/γ'共晶的比例显著增加，而下表面则减少。在抽拉速率降低时，γ/γ'共晶向上聚集变得更为严重。同时，样品中Al+Ta的百分比与γ/γ'共晶的比例呈正相关。Al和Ta元素在凝固前沿中的热-溶质对流是导致共晶非均匀分布的主要原因。即使经过后续的固溶热处理，也不能消除γ/γ'共晶的非均匀分布，导致上表面共晶超标并最终致使叶片报废。

关键词：镍基单晶高温合金；共晶；抽拉速率；热-溶质对流

作者简介：赵运兴，男，1988年生，博士，中南大学粉末冶金国家重点实验室，湖南 长沙 410083，E-mail：zhaoyunxing@csu.edu.cn